



NiTi–Al interface strength in ultrasonic additive manufacturing composites



Ryan Hahnlen, Marcelo J. Dapino^{*}

Smart Vehicle Concepts Center, Department of Mechanical and Aerospace Engineering, The Ohio State University, 201 W 19th Ave., Columbus, OH 43210, United States

ARTICLE INFO

Article history:

Received 10 July 2012

Received in revised form 26 September 2013

Accepted 25 October 2013

Available online 9 December 2013

Keywords:

A. Metal-matrix composites

B. Fibre/matrix bond

C. Analytical modeling

D. Mechanical testing

Shape memory alloys

ABSTRACT

Ultrasonic Additive Manufacturing (UAM) is a new rapid prototyping process for creating metal-matrix composites at or near room temperature. The low process temperatures enable composite materials that have tailored CTEs through utilizing recovery stresses generated by highly prestrained Shape Memory Alloy (SMA) fibers embedded within the matrix. The strength of the fiber-matrix interface, which is the limiting factor in UAM composites, has not been characterized. In this study, we characterize the shear strength of the fiber-matrix interface and study the bonding between the fiber and matrix in composites fabricated with prestrained NiTi embedded in an Al 3003-H18 matrix. In heating the composite, stresses develop due to the blocked behavior of NiTi and the difference in CTE of the matrix and fiber. Differential scanning calorimetry is used to observe composite failure temperatures; an average interface shear strength of 7.28 MPa is determined using constitutive models of the NiTi element and Al matrix. The constitutive models describe the thermally-induced strain of the composite, showing an effective CTE of zero at 135 °C. The models show that by increasing the embedded fiber length, interface failure temperatures can be increased so that zero CTE behaviors can be utilized without irreversibly changing the NiTi prestrain. Results from energy dispersive X-ray spectroscopy indicate that the bonding between the fiber and interface is mechanical in nature with no evidence to support chemical or metallurgical bonding.

© 2013 Elsevier Ltd. All rights reserved.

1. Introduction

Shape Memory Alloys (SMAs) have unique properties that make them attractive for creating multifunctional structures. SMAs are commonly utilized for their characteristic strain recovery but they can also generate significant recovery stresses when heated in a constrained state [1,2]. By utilizing the temperature dependent recovery stresses of a prestrained SMA element, it is possible to construct an SMA composite that can offset the thermally-induced strain of the composite matrix along the fiber direction. In this composite, though both the SMA and matrix are subject to linear thermal expansion, a compressive load is applied to the composite matrix as recovery stress in the SMA increases with temperature. Along a given direction, the total strain reaction of the composite is dependent upon the elastic moduli and CTE of the matrix and SMA fiber, the fiber volume fraction, and the prestrain level of the SMA. The cross-sectional shape of the SMA fiber has an indirect effect: given composites with identical SMA volume fractions but with different cross sectional shapes, the interface area between the SMA and matrix will be different. This will not impact the over-

all behavior of the composite but will affect the load the interface can withstand without failing.

This study considers metal-matrix composites consisting of an Al 3003-H18 matrix and shape memory NiTi fiber fabricated through Ultrasonic Additive Manufacturing (UAM), a rapid prototyping technology based on ultrasonic metal welding. In this process, two workpieces are held together under a compressive load and ultrasonically vibrated relative to one another. The motion creates a friction-like action that disrupts surface oxides and shears surface asperities, creating nascent surfaces [3,4]. The compressive load applied to the pieces causes opposing clean metal surfaces to form bonds, thus joining the two components. During UAM, illustrated in Fig. 1(a), the ultrasonic vibrations are generated by piezoelectric transducers and transmitted to the workpieces through tuned waveguides and a rolling sonotrode which is specially textured to grip the top workpiece. While metallic bonding is often cited as the bonding mechanism between workpieces of similar alloys [3–9], the bonding mechanisms for dissimilar materials joined via UAM have been identified as mechanical interlocking, friction, and in some cases, metallurgical bonding [6,10–14]. The primary benefit of UAM is that pieces are consolidated at room temperature and macro-scale heating does not noticeably raise the temperature of the bulk composite. This aspect is critical for

^{*} Corresponding author.

E-mail address: dapino.1@osu.edu (M.J. Dapino).

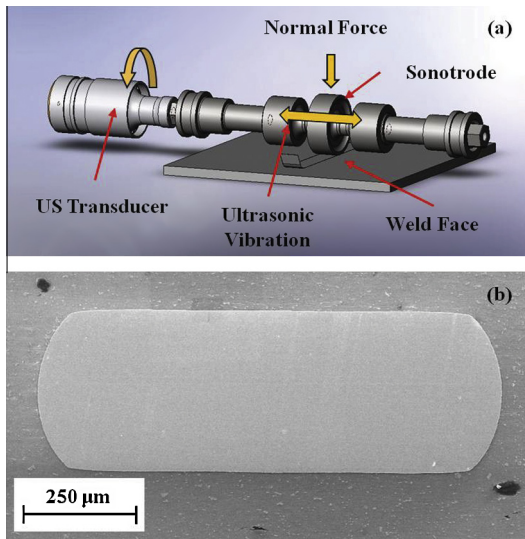


Fig. 1. (a) In the UAM process, successive layers of metal tape are bonded together to create metallic composites with embedded materials. (b) Cross section of an NiTi–Al composite with 254 μm by 762 μm NiTi ribbon.

SMA metal-matrix composites as excessive heating, such as in powder metallurgy or casting processes, can change the prestrain level via transformation and alter the stable characteristic behavior of the SMA [15–18].

Both the recovery stresses generated by the prestrained NiTi and relatively large CTE of the Al matrix cause significant stresses to develop with increasing temperature at the interface of the fiber and matrix. The strength of the interface is of particular significance as if it fails, the NiTi fibers will be allowed to recover any induced prestrain through the transformation from detwinned martensite to austenite (M–A) and thus will not generate recovery stresses upon subsequent heating cycles.

In this study, UAM NiTi–Al composite samples are created with highly prestrained NiTi ribbon. The composites are used to determine the interface failure and to study the nature of the bonding mechanism between NiTi and Al. For the purpose of this paper and the discussion herein, prestrain is defined as the amount of strain the NiTi elements exhibit due to the detwinning of martensite, excluding strain due to thermal expansion, elastic loading, and plastic deformation. The prestrain is critical because it creates the stress-induced martensite variant in the SMA. If the SMA element is left unconstrained, the induced prestrain will be recovered as the detwinned martensite transforms to austenite upon heating. If the SMA element is constrained, the transformation is inhibited and recovery stresses develop due to elastic loading of the constraint as the restricted transformation recovers a small amount of the prestrain [1,19]. If there is no initial prestrain in the SMA, the phase at room temperature is twinned martensite, also called self accommodating or temperature-induced martensite. Transformation from twinned martensite to austenite will not induce strain recovery, as there is no detwinning strain to recover, and therefore will not generate recovery stresses if the SMA element is constrained. Since the matrix cannot support the full strain recovery of the detwinned SMA, as much as 6%, interface failure is coincident with the M–A transformation of the embedded NiTi.

The interface failure can be detected by Differential Scanning Calorimetry (DSC), an established method for observing behavior and failure in SMA-epoxy based composites [20–22]. The DSC measurement can identify the temperature range over which the M–A transformation occurs. This is observed as a negative power peak since the M–A transformation is an endothermic process. Because

the transformation from detwinned martensite to austenite recovers the prestrain induced by detwinning the martensitic phase, the DSC transformation peak also signifies the recovery of the induced strain in the SMA element. Due to the constraint of the matrix, the strain recovery can only take place if the ribbon-matrix interface is compromised, releasing the constraint on transformation, or if the matrix or ribbon are stressed beyond their yield strength, allowing the strain to be recovered through plastic deformation of the materials. Creep or stress relaxation is not considered as a mechanism for strain recovery since the temperatures are relatively low as are times during DSC tests. In this study, DSC is used to identify the M–A transformation and concurrent strain recovery of the NiTi ribbons in NiTi–Al composites. An SMA-composite model is then used in conjunction with known material properties, composite parameters, and temperature to determine stresses in the NiTi and Al composite components at failure and to derive the interface strength of NiTi–Al UAM composites. The determined interface strength serves as an important design parameter in future NiTi–Al composites and serves as a baseline value for future investigations in which interface strengthening methods will be studied.

The mechanism for load transfer across the interface is determined using Energy Dispersive X-ray Spectroscopy (EDS). EDS allows investigation of the region near the NiTi–Al interface to determine how material composition varies as a function of distance from the interface. If a solid-state bond exists between the NiTi and Al, two indicators are expected: a removal of surface oxides and possible diffusion of elements across the interface boundary. Both of these are observable through EDS.

2. Procedures

Prior to embedding, the NiTi ribbon was first heated in a stress-free state to transform any detwinned martensite in the as-received material and allowed to cool stress-free to room temperature to ensure the ribbon was fully twinned (temperature-induced) martensite. The ribbon was next fully detwinned by applying a 36 N dead weight resulting in a tensile stress of 186 MPa, three times greater than the observed critical finish stress, σ_{cr}^f , of this alloy at room temperature.

The critical finish stress and other material properties of the SMA were obtained through thermomechanical testing on material from the same lot as the embedded NiTi. Included in Table 1 are the austenite transformation temperatures (A_s and A_f), martensite transformation temperatures (M_s and M_f), stress influence coefficient for the austenite transformation temperatures (C_A), and the critical finish stress. The austenite start temperature

Table 1

Material properties used for composite analysis. Unless cited, values were found experimentally.

Property	Description	Value
E_M	Martensite modulus	17.9 GPa
E_A [24]	Austenite modulus	83 GPa
$E_{Al}(24^\circ\text{C})$ [27]	Al modulus at 24 $^\circ\text{C}$	68.3 GPa
$E_{Al}(100^\circ\text{C})$ [27]	Al modulus at 100 $^\circ\text{C}$	65.5 GPa
α_{Al} [27]	Al 3003 CTE	23.2 $\mu\text{e}/^\circ\text{C}$
α_{NiTi} [26]	NiTi CTE	10 $\mu\text{e}/^\circ\text{C}$
A_s	Austenite start temp.	45 $^\circ\text{C}$
A_f	Austenite finish temp.	60 $^\circ\text{C}$
M_s	Martensite start temp.	45 $^\circ\text{C}$
M_f	Martensite finish temp.	41 $^\circ\text{C}$
C_A	Stress influence coeff.	8.1 MPa/ $^\circ\text{C}$
ϵ_L	Max. recoverable strain	–6%
σ_{cr}^f	Crit. finish stress at 24 $^\circ\text{C}$	62 MPa
σ_y^{NiTi}	NiTi yield str.	816 MPa
σ_y^{Al} [28]	Al 3003 comp. yield str.	140 MPa

is the temperature at which the M–A transformation begins when the NiTi sample is under no stress. Similarly, A_f is the temperature at which the M–A transformation is complete in the absence of stress. Upon stress-free cooling, the A–M transformation occurs over the temperature range between M_s and M_f . Since the cooling behavior of the composites is not studied in this research, the martensite transformation temperatures are provided only for completeness. The transformation temperatures are generally considered linearly dependent with stress through [23]

$$A_s^\sigma = A_s + \sigma/C_A, \quad (1)$$

and

$$A_f^\sigma = A_f + \sigma/C_A. \quad (2)$$

The critical finish stress is the stress at which all twinned martensite has been converted to detwinned martensite at room temperature. For the NiTi ribbon used in this study, the critical finish stress, yield strength (σ_y), elastic modulus of martensite (E_M), and maximum recoverable strain (ϵ_r) were found through stress–strain tests conducted at room temperature. The stress influence coefficient was found through blocked force testing and transformation temperatures were found through a combination of DSC tests, electrical resistivity tests, and thermally-induced strain tests. These measurements are in agreement with manufacturers' data as well as that of other researchers [24–26].

A first NiTi–Al composite was fabricated by consolidating two 150 μm thick Al 3003-H18 strips onto an Al baseplate using a custom 9 kW UAM system. Next, a rectangular NiTi ribbon, 254 μm thick by 762 μm wide, was placed on the surface and two additional Al tapes were welded over top, encapsulating the ribbon as shown in the cross section in Fig. 1(b). During consolidation, the NiTi ribbon was clamped in place outside of the weld area to prevent ribbon movement. After consolidation, the composite was machined to achieve its final width, 1.8 mm, and remove the base plate. From the resulting composite, three samples were cut to length for DSC testing using a lubricated low speed diamond precision saw to avoid heating and transformation of the NiTi ribbon. The finished samples have an average NiTi fiber volume fraction of 15.1%. A second composite was sectioned and polished for EDS analysis to study the NiTi–Al interface. This sample was also sectioned using a low speed diamond precision saw. After cutting, all samples were cleaned in methanol to remove any contaminants.

In preparation for DSC analysis, each sample was placed in an Al test pan while a single empty test pan was used as a comparative reference for all measurements. Two heating cycles were recorded during DSC measurement for each sample. During both cycles, temperature was increased at a rate of 10 $^\circ\text{C}/\text{min}$. Cooling was augmented by compressed air between cycles but was not recorded. DSC sample 1 was examined in a Scanning Electron Microscope (SEM) after testing to observe the NiTi–Al interface.

The polished section of the second NiTi–Al composite was analyzed via EDS to observe compositions across the NiTi–Al interface. EDS line scans were conducted at the top and bottom interfaces between the NiTi ribbon and Al matrix, shown in Fig. 2, the most likely sites for metallic bonding between the composite components. Scans consisted of point measurements no more than 0.8 μm apart with an electron accelerating voltage of 20.0 kV. If bonding between NiTi and Al does occur during the UAM process, two key observations are expected. First, for metallic bonding to occur, the oxide layers of both workpieces must be removed. Second, diffusion may also occur with metallic bonding and thus, elements from the matrix and embedded SMA, namely Ni, Ti, and Al, are expected to migrate across the interface if such bonding is present. In the conducted line scans, the atomic percentage of Al,

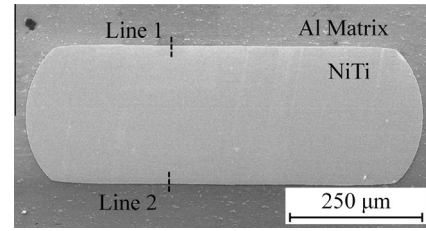


Fig. 2. Image of NiTi–Al composite 2 showing locations of lines for EDS analysis.

Ni, Ti, and O were recorded at each point in the scan and plotted as a function of distance from the interface.

3. Experimental results and discussion

The behaviors observed in DSC for all samples are similar. Both thermal cycles of sample 2 are compared in Fig. 3, showing the differential power needed to heat the composite and the reference pan to the same temperature, as a function of temperature. The endothermic peaks and associated decreases in differential power observed in both cycles indicate the M–A transformation of the embedded NiTi ribbons. Five key regions are identified in the first cycle and are defined by either consistent behavior or transition points between areas of different behavior. Region (i) is the initial state, characterized by the stabilization of the differential power measurement from the DSC system. Region (ii) is characterized by a nearly horizontal power versus temperature relationship. Region (iii) is defined by the negative power–temperature slope prior to the endothermic transformation peak. Region (iv) is noted as the transition between region (iii) and the low temperature portion of the endothermic peak at temperature T_x . Region (v) is the intersection of linear interpolations of the high temperature portion of the endothermic transformation peak and the consistent behavior at higher temperature characterized by an approximately horizontal differential power versus temperature curve.

An interpretation of the composite behavior at each region is shown in Fig. 4. It is noted that the Al alloy comprising the matrix

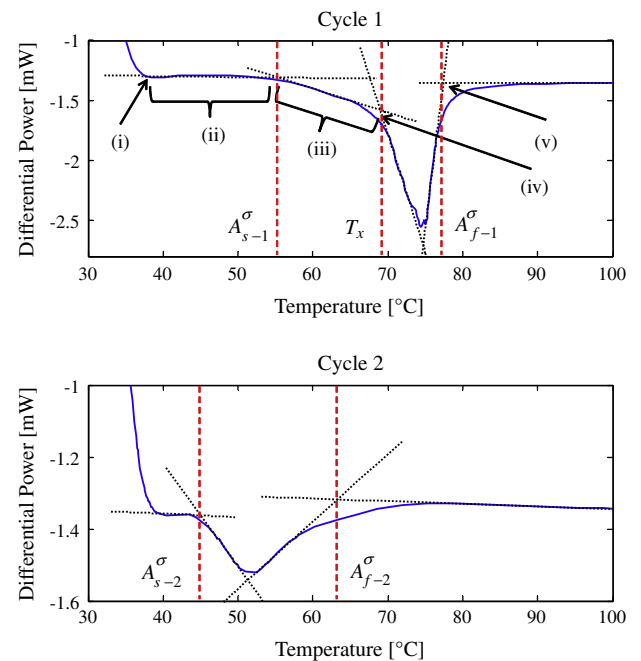


Fig. 3. DSC heating cycles 1 and 2 of sample 2.

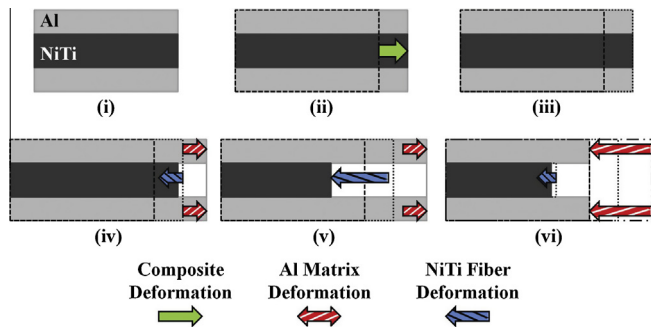


Fig. 4. Physical representation of DSC regions: (i) reference state; (ii) linear thermal expansion of total composite; (iii) reduced expansion due to generation of recovery stresses; (iv) NiTi–Al interface failure; (v) NiTi transformation complete; (vi) cool to reference temperature (not plotted in Fig. 3).

does not undergo any phase changes over the test temperature range and the samples were cleaned prior to testing. Any deviations from a constant power versus temperature curve are related to the transformation of the embedded NiTi ribbons. All behaviors are described relative to the reference state in region (i). Through region (ii), linear thermal expansion of the total composite is occurring. In region (iii), the temperature has surpassed the composite austenite start temperature, A_{s-1}^{σ} . As the composite temperature increases, the NiTi ribbon generates a recovery stress as a function of temperature which is resolved as a compressive load on the Al matrix. The elastic deformation of the matrix due to the recovery stress allows a partial transformation to occur. This results in an apparent reduction in CTE of the composite. At region (iv) the generated stresses overcome the shear strength of the NiTi–Al interface and transformation of the detwinned martensite begins unconstrained. Once the constraint of the matrix is relieved, the M–A transformation occurs more rapidly with respect to temperature as indicated by the larger magnitude of the power–temperature slope after region (iv). As the NiTi ribbon transforms it recovers the induced prestrain, contracting within the Al matrix. In regions where the interface has separated, the Al matrix is able to freely expand via thermal expansion. At region (v) the NiTi transformation and strain recovery are complete and the original interface between the fiber and matrix has completely failed due to the strain recovery. A new mechanical interface now exists at the new contact points between the fiber and matrix. Further heating results in linear thermal expansion of the composite. Region (vi), not recorded in the DSC tests, is thermal contraction of the composite during cooling. While the NiTi ribbon has contracted within the Al matrix, there is still friction between the ribbon and matrix which allows load transfer, the friction governs the thermomechanical properties of the composite in subsequent cycles.

Using the intersection of linear interpolations of the identified regions, several important temperatures are determined. The intersection of regions (ii) and (iii) is taken as the initial austenite start temperature, A_{s-1}^{σ} , as previously noted. This temperature is higher than the austenite start temperature of the ribbon, A_s , due to thermoelastic stress arising from the different CTEs of Al and NiTi as well as a preload due to manufacturing to be discussed momentarily. The temperature at region (iv), denoted T_x , represents the onset of the NiTi–Al interface failure. Region (v) denotes A_{f-1}^{σ} , the temperature at which the M–A transformation is complete. At this temperature all prestrain has been recovered and further increases in temperature do not affect the NiTi phase. The presence of the endothermic peak in cycle 1, ending at region (v), indicates the M–A transformation has occurred, simultaneously causing the recovery of prestrain. Once the prestrain is recovered, there is no mechanism to reintroduce the 6% strain upon cooling; the composite has undergone a functional failure.

The second thermal cycle in Fig. 3 shows a shift in the endothermic peak and transformation temperatures, A_{s-2}^{σ} and A_{f-2}^{σ} , to nearly the stress-free transformation temperature values for this alloy as listed in Table 1. The austenite start temperature of cycle 2 is lower than that of cycle 1, indicating that there was a persistent preload on the NiTi ribbon after embedding. This preload is likely due to a combination of tension developed during the clamping process and the rolling action of the sonotrode imparting a tensile load during embedding. Further, cycle 2 does not exhibit a temperature range analogous to region (iii) in which recovery stresses were generated in the initial cycle. As a result, A_{f-2}^{σ} is significantly lower than A_{f-1}^{σ} due to the absence of blocking stresses generated at temperatures above A_{s-2}^{σ} [29]. This is supporting evidence that all prestrain was recovered in the first cycle due to failure of the interface. The temperatures of interest for all 3 samples are given in Table 2. Also provided in Table 2 are the transformation enthalpies for both cycles of the samples. Cycle 1 in all cases has significantly more enthalpy than cycle 2. This difference is attributed to strain transformation, matrix constraint, and interface failure, all of which are present in the first cycle and require more energy to complete the M–A transformation. With no strain recovery in cycle 2 and very little constraint by comparison, the M–A transformation does not require as much energy and as a result, has a lower transformation enthalpy.

NiTi–Al DSC sample 1 was removed from the test pan, rinsed in methanol, and placed in an SEM for a post-failure inspection of the interface. Representative images of the interface are shown in Fig. 5. Separation between the NiTi and Al matrix can be seen around the perimeter of the NiTi ribbon indicating that there was mechanical failure of the interface. Further, the insets of Fig. 5(a) and (b) show a line in the Al matrix running parallel to the NiTi ribbon boundary. This line is the edge of the Al matrix; the region between the NiTi and the line in both images is the interior interface surface exposed due to contraction of the ribbon during transformation and failure.

The change in atomic percent of elemental composition across the NiTi–Al interface for EDS lines 1 and 2 are shown in Fig. 6. While EDS line scan points were taken at intervals of approximately 1 μm , the resolution of the measurement is also dependent upon the electron interaction radii of the material being scanned. A Monte Carlo simulation of electron flight paths estimated interaction radii for Al and NiTi of 2.6 μm and 1.2 μm , respectively. The result of the interaction radii is that the EDS results will show a transition equal to the sum of the radii, 3.8 μm , as a scan transitions through a perfect, diffusionless interface between Al and NiTi. In considering the EDS results, a transition region greater than 3.8 μm will indicate the presence of diffusion while a transition less than or equal to 3.8 μm will indicate that there is no measurable diffusion between the materials.

Line scan 1 shows the Al to NiTi transition occurring over 3.0 μm while line 2 has a transition of 3.3 μm , both of which are

Table 2

Transformation temperatures, failure temperature, NiTi stress at failure, and interface shear strength for samples 1, 2, and 3. Note: σ_x and τ_f are stresses calculated using (7) and (11) presented in Section 4.

Parameter	Sample 1	Sample 2	Sample 3
A_{s-1}^{σ} [°C]	55.5	55.5	56.4
A_{f-1}^{σ} [°C]	77.7	77.4	77.5
A_{s-2}^{σ} [°C]	44.5	45.0	44.7
A_{f-2}^{σ} [°C]	62.6	63.2	60.0
T_x [°C]	69.2	69.0	68.4
ΔH_1 [J/g]	18.6	24.0	23.6
ΔH_2 [J/g]	0.5	1.7	0.7
σ_x [MPa]	177	175	171
τ_f [MPa]	7.61	7.02	7.23

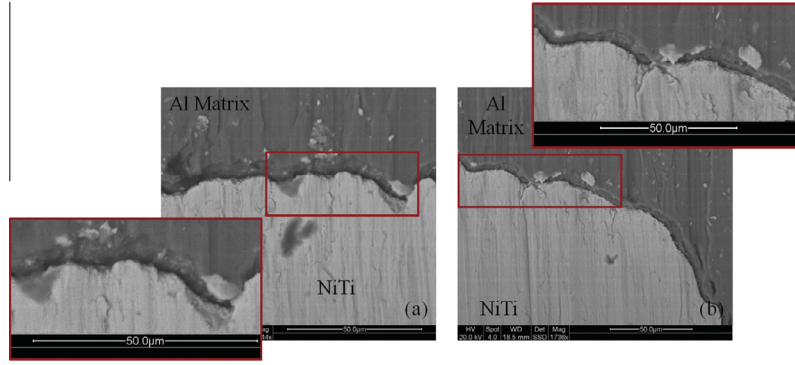


Fig. 5. Representative SEM images of DSC sample 1 showing evidence of debonding and ribbon contraction: (a) NiTi–Al interface along flat region showing interface separation and interior surface of the Al matrix; (b) NiTi–Al interface on ribbon corner showing interior surface of the Al matrix.

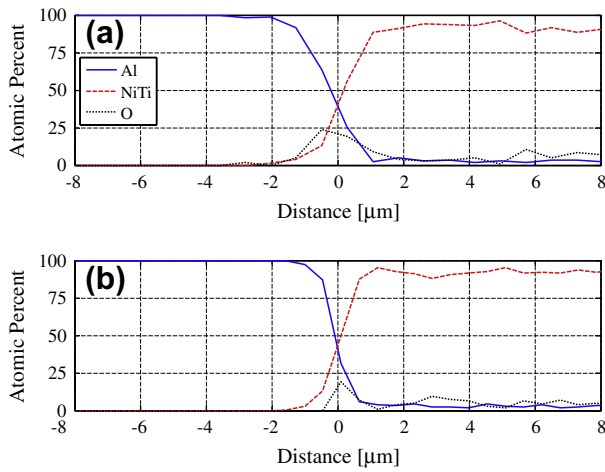


Fig. 6. EDS results for NiTi–Al composite 2: (a) line scan 1; (b) line scan 2.

below the threshold for measurable diffusion indicating that there is no diffusion based bonding between the NiTi and Al constituents. Further, in both line scans there is a peak in oxygen content as the Al and NiTi composition lines intersect. This indicates that at least one oxide layer is still present at the interface. A key aspect to bonding via UAM is the removal of surface oxide at the interface of the workpieces. From the EDS results, the ultrasonic vibrations generated for the consolidation process were not sufficient to create nascent surfaces at the NiTi–Al interface, thus making a metallurgical bond unlikely. While metallurgical bonding between NiTi and Al is doubtful, the SEM image in Fig. 2 shows very close contact around the entire perimeter of the NiTi ribbon cross section indicating that friction is the primary means of load transfer between the matrix and ribbon. From the EDS results, it may be possible to increase the strength of the interface by removing the oxide layer on the Al tapes and NiTi ribbons prior to embedding as a way to promote solid-state bonding. Further, by texturing the ribbon, mechanical interlocking and additional surface area can be increased leading to a subsequent increase in friction-based interface strength.

4. Modeling

To model the response of the samples to temperature changes, a strain matching method, similar to models used for SMA-epoxy composites [30–32], was employed. Under the condition that the interface remains intact, the strain in the fiber direction is identical for the Al matrix and NiTi ribbons. The Al and NiTi strains can be

expanded into their constituent components for mechanical, thermal, and transformation strains,

$$\epsilon_{Al} = \frac{1}{E_{Al}}(\Delta\sigma_{Al}) + \alpha_{Al}(\Delta T), \quad (3)$$

and

$$\epsilon_{NiTi} = \frac{1}{E_{NiTi}}(\Delta\sigma_{NiTi}) + \alpha_{NiTi}(\Delta T) + \epsilon_L(\xi_s - \xi_{so}), \quad (4)$$

where $\Delta\sigma$ is the change in total stress from the initial state, ΔT is the total temperature change, E is the elastic modulus, α is the CTE, ξ_s is the stress-induced martensitic volume fraction, ξ_{so} is the initial stress-induced martensitic volume fraction, and ϵ_L is the maximum recoverable strain of NiTi.

The martensitic volume fraction, ξ , is a state variable that describes the phase of the SMA. When the SMA is fully martensitic (either stress or temperature-induced), $\xi = 1$. When the SMA is fully austenitic, $\xi = 0$. The stress-induced martensitic volume fraction is a subset of the total martensitic volume fraction such that [23]

$$\xi = \xi_s + \xi_T, \quad (5)$$

where ξ_T represents the temperature-induced martensitic volume fraction. In the context of this study, the fully prestrained NiTi ribbons have the maximum amount of detwinned martensite and therefore have $\xi = \xi_s = 1$ prior to the first heating cycle. If the prestrain is recovered after the first heating as hypothesized, the ribbons are fully temperature-induced martensite where $\xi = \xi_T = 1$ ($\xi_s = 0$) prior to the start of the second heating cycle.

During heating, no external load is applied; the composite is allowed to freely expand or contract as the temperature changes. Force balance is used to obtain the stress in the Al matrix in terms of NiTi stress,

$$\Delta\sigma_{Al} = \frac{-f}{(1-f)} \Delta\sigma_{NiTi}, \quad (6)$$

where f is the fiber volume fraction. The stress in the ribbon can be obtained as a function of temperature, material properties, volume fraction, and NiTi transformation terms by substituting (6) into (3), equating to (4), and solving for $\Delta\sigma_{NiTi}$,

$$\Delta\sigma_{NiTi} = \frac{(\alpha_{Al} - \alpha_{NiTi})(\Delta T)}{\frac{1}{E_{NiTi}} + \frac{1}{E_{Al}} \frac{f}{(1-f)}} - \frac{\epsilon_L(\xi_s - \xi_{so})}{\frac{1}{E_{NiTi}} + \frac{1}{E_{Al}} \frac{f}{(1-f)}}. \quad (7)$$

This equation has two components: a thermoelastic component which any composite exhibits if a CTE mismatch exists between the fibers and matrix, and a component due to the transformation-induced strain recovery of NiTi embedded in a detwinned state ($\xi_{so} \neq 0$). If the embedded NiTi elements are not prestrained before

construction or if the temperature is below A_s^σ , only the thermoelastic stress component remains. If $\Delta\sigma_{NiTi}$ is expanded to $\sigma_{NiTi} - \sigma_{NiTi0}$, where σ_{NiTi0} is the initial stress on the ribbons, (7) can be rearranged to provide

$$\sigma_{NiTi} = \frac{(\alpha_{Al} - \alpha_{NiTi})(\Delta T)}{\frac{1}{E_{NiTi}} + \frac{1}{E_{Al}} \frac{f}{(1-f)}} - \frac{\epsilon_L(\xi_s - \xi_{s0})}{\frac{1}{E_{NiTi}} + \frac{1}{E_{Al}} \frac{f}{(1-f)}} + \sigma_{NiTi0}, \quad (8)$$

indicating that any preload prior to heating can be treated as a stress offset. This has implications regarding the preload due to manufacturing as discussed below.

The martensitic volume fractions are found through equations based upon the Brinson constitutive SMA model [23]. Since the samples were in a detwinned martensite state for a single heating cycle, only the M–A transformation is considered. For the M–A transformation the martensitic volume fraction is given by

$$\xi = \frac{\xi_0}{2} (\cos [a_A(T - A_s^\sigma)] + 1), \quad (9)$$

where

$$a_A = \frac{\pi}{A_f - A_s}. \quad (10)$$

This transformation only occurs when $A_s^\sigma < T < A_f^\sigma$ and as the composite temperature is increasing. In the case of the test samples, the total martensitic volume fraction, ξ , consists of stress-induced martensite with $\xi_s = \xi = 1$ assumed to hold true for the entirety of the first heating cycle. The elastic modulus of NiTi is calculated using a rule of mixtures as a function of the martensitic volume fraction. The modulus of the matrix is calculated using linear interpolation of the elastic modulus value at room temperature and 100 °C. For the first and second heating cycles, the SMA is assumed to start from a fully martensitic state, $\xi_0 = 1$. If a thermal cycle is initiated when the SMA phase is in a mixed phase, $0 < \xi_0 < 1$, there will be minor effects on the thermoelastic response as the higher austenite modulus will increase stress on the ribbon during heating, thus slightly increasing the effective transformation temperatures through (1) and (2).

Stress and volume fraction are calculated for a prescribed temperature to obtain the stress–temperature load profile for the initial heating cycle shown in Fig. 7(a). The plot shows two load paths: a profile in which the embedded NiTi has no initial preload and a profile that was made to intersect A_s^σ at the average A_{s-1}^σ temperature of 55.8 °C. Both modeled cases have a stress-induced martensite volume fraction of 1, and therefore have the same amount of prestrain. The varied preload takes into account the amount of tensile stress applied to the SMA ribbon after it has been detwinned. Due to the transformation temperatures of this alloy and the stress–strain relationship of SMAs, the ribbon can be given a 6% prestrain and be unloaded to a zero preload condition while maintaining the prestrain level due to the formation of detwinned martensite. Further, once fully detwinned, additional tensile loads will change preload without changing the prestrain value associated with detwinning. This model suggests that the NiTi ribbon was under a 86.3 MPa preload during embedding. It is noted that the zero preload profile begins the M–A transformation at 45.6 °C, close to the average A_{s-2}^σ temperature of 44.7 °C, indicating that the embedded ribbons have recovered all prestrain and preload after the initial DSC cycle. The A_{f-2} temperatures are also close to the stress free A_f temperature for the alloy given in Table 1, indicating no initial prestress or significant generation of blocking stress that would occur if stress-induced martensite was still present. The stress–temperature load profile with the 86.3 MPa preload was used to determine the stress in the NiTi at interface failure, when $T = T_x$. The average interface failure temperature, 68.9 °C,

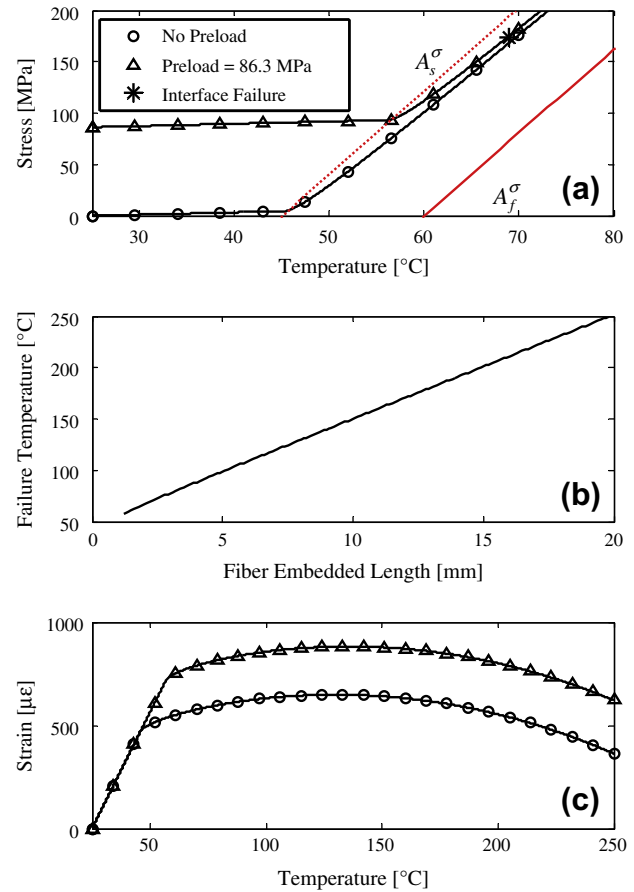


Fig. 7. Model of NiTi–Al composites: (a) stress versus temperature; the asterisk marks interface failure; (b) interface failure temperature as a function of embedded fiber length; (c) strain versus temperature.

is marked by an asterisk in the phase diagram. The associated NiTi stress is 174 MPa.

This stress can be used to calculate the maximum stress in the Al matrix using (6). Assuming an average NiTi fiber volume fraction of 15.1%, the stress applied to the Al matrix is 31 MPa in compression. Comparing the 174 MPa NiTi tensile stress and 31 MPa Al compressive stress to their respective yield strengths given in Table 1, it is clear that the change in temperature during the DSC trial was not sufficient to cause plastic deformation of either constituent. The only other mechanism to allow transformation and subsequent strain recovery of the NiTi in the first DSC cycle is failure and separation of the NiTi–Al interface, which is supported by the post-failure SEM observations.

Once failure is initiated at T_x , the NiTi and Al stress will immediately begin to diminish as the constraint and thermoelastic stresses generated by the Al matrix are no longer fully acting on the ribbons. As a result, the effective austenite finish temperature, as calculated through (2), drops after failure. If the composite did not fail through prestrain recovery, the A_f^σ temperature would remain high due to the increasing blocking stress. This is visualized by continuing to follow the stress–temperature load paths in Fig. 7(a) beyond the asterisk. The load path will not intersect the A_f^σ line until 597 °C and 4350 MPa. It is noted that reaching these levels of temperature and stress is unlikely as other factors including yielding of the materials would contribute to failure of the composite prior to transformation completion. However, the fact that transformation ends in the first DSC cycle at an average value of 77.5 °C indicates that NiTi stress has been significantly relieved. Further, the shift in transformation temperatures in cycle 2 indi-

cates an irreversible change has occurred and the composite has undergone a functional failure via prestrain recovery.

In considering the UAM samples, it is assumed that there is no metallurgical bonding between the NiTi and Al as ultrasonic welding times are short and temperatures are not high enough to support diffusion [13]. This is supported by the EDS results that show no measurable diffusion and a persistent oxide layer that would inhibit the formation of a solid state bond. Load transfer is believed to be due to friction between the constituent components. The shear strength of the NiTi–Al interface is calculated by

$$\tau_f = \sigma_x A_{\text{NiTi}} / A_{\text{shear}}, \quad (11)$$

where σ_x is the NiTi stress at T_x calculated from (7), A_{NiTi} is the ribbon cross sectional area, and A_{shear} is the interface surface area. The average interface shear strength was found to be 7.28 MPa. The maximum NiTi stress and interface shear strength for all samples are presented in Table 2.

Interfacial shear strength due to friction between the fiber and matrix is not dependent upon the fiber length [33] and neither is the blocking force generated by the NiTi element. However, the shear stress generated by the blocking force is dependent upon ribbon surface area which is proportional to fiber length. This implies that as composite length increases for similar NiTi–Al composites, so will failure temperature, eventually reaching a point where composite failure may occur through yielding of the NiTi elements, compressive yielding of the Al matrix, or buckling of the composite rather than interfacial failure. The developed model is utilized to calculate failure temperatures of similar composites based upon the length of the embedded ribbon. Using prescribed lengths and proportional shear areas, the NiTi stresses required to surpass the interface shear strength are determined. The required stresses to induce interface failure have unique failure temperatures which are plotted in Fig. 7(b). The plot accounts for the effect of the preload estimated in the DSC samples, however the difference between the failure temperature with and without preload is less than 1 °C. With 86.3 MPa preload, the minimum length is 1.2 mm. Below this length, the stresses applied by the elastic preload are sufficient to cause interface failure without heating.

From Fig. 7(b), a composite with a length of 20 mm has a sufficiently large shear area to be heated to 250 °C before interface failure. The implications of increasing the fiber length, and therefore operating temperature range, are demonstrated in the modeled strain-temperature behavior of these composites, shown in Fig. 7(c). By substituting the NiTi stress calculated by (7) into (4), a plot of strain versus temperature is obtained. Both the zero preload and 86.3 MPa preload conditions are shown in Fig. 7(c). At temperatures below A_s^0 , the thermally-induced strain will follow a linear path while temperatures beyond A_s^0 will cause the effective composite CTE to decrease substantially as a result of recovery stresses generated by the detwinned NiTi ribbon. The strain-temperature model indicates that if the NiTi ribbon is not embedded under a preload, the strain will reach a maximum and have an effective CTE of zero at 130 °C while a preload similar to the tested samples will cause the strain maximum and zero CTE point to occur at 135 °C. By varying the NiTi fiber volume fraction, the prestrain level, and ribbon preload, the thermally-induced strain response can be tailored to have a near zero CTE over a defined temperature range. In addition, by selecting a shape memory alloy with lower transformation temperatures, the linear strain region can be eliminated at room temperature. While interface failure can be avoided by increasing the embedded fiber length, failure of the matrix or fiber is a concern as stress continues to increase with temperature. With a sufficiently long embedded fiber, the temperature at which the matrix or fiber fails will be the limiting temperature of the composite. To illustrate, a composite of similar construction is considered, including a 15.1% fiber

volume fraction, 86.3 MPa persistent tensile preload on the fiber at room temperature, and a length sufficient to avoid interface failure. Using (8) and (9) and the yield strength of NiTi provided in Table 1, the stress generated within the composite will exceed the tensile yield strength of the NiTi ribbon, 816 MPa, at 151 °C. Similarly, using (6) to equate (8) to σ_{Al} , the matrix stress will exceed the compressive yield strength of Al 3003, 140 MPa, at 148 °C. Yielding of one component will allow the NiTi fiber to recover a significant amount of prestrain, thus irrevocably changing the composite behavior upon further thermal cycling. In this particular case, the yield strength of the Al matrix will be reached first, limiting the low CTE behavior to below 148 °C. Note that stress in the Al matrix and stress in the NiTi fiber are related through (6) and therefore the component that fails first is determined solely by the fiber volume fraction.

If maximum service temperatures or composite lengths are selected such that the matrix and fiber do not yield and the interface failure temperature is not reached, the composites are expected to have a repeatable thermomechanical behavior. For prestrained shape memory NiTi, this would include a thermoelastic region followed by a reduced CTE region due to the generation of blocking stress. Upon cooling, the prestrain would be reintroduced into the SMA as it cools between M_s and M_f by loading from the Al matrix. Below M_f , the SMA prestrain would be maintained and thus further heating would produce similar results for subsequent cycles. Such repeatable behavior is imperative if similar builds are to be used as the basis of SMA composite components.

5. Conclusions

In this research, interface failure of NiTi–Al UAM composites was observed through DSC and modeled using the known behavior of the embedded SMA material. The nature of the NiTi–Al interface bond was also examined through EDS analysis. Using the DSC results and composite model, the interfacial shear strength was determined. Failure temperature was consistent between all samples with an average of 68.9 °C. Using the developed constitutive composite model, the average shear strength of the interface was found to be 7.28 MPa. While the interfacial shear strength and the blocking force are not dependent upon length of the embedded NiTi elements, the shear stress at the interface is inversely proportional to ribbon length. This suggests that by increasing the composite length the interface failure temperature is increased significantly, avoiding irrecoverable composite damage. EDS analysis indicates there is no solid state or metallurgical bonding due to a persistent oxide layer and no measurable diffusion across the NiTi–Al interface. This provides two additional avenues for strengthening the interface. First, it may be possible to promote metallurgical bonding through oxide layer removal prior to embedding. Another possible way to increase interface strength would be to increase surface area through a textured surface on the NiTi ribbon. Ultimately, composite failure may not be limited by interface strength, but instead by material yield strengths and critical buckling loads. By increasing the failure temperature through interface strengthening or increasing shear area, this process can be used to create composite systems that have low effective CTEs over a wide temperature range. By having an aluminum based structure with a low CTE, significant weight saving can be made over structures created using iron based alloys with similar thermal expansion properties.

Acknowledgments

The authors would like to acknowledge Mark Norfolk and Karl Graff from the Edison Welding Institute for their assistance and

use of UAM equipment as well as Phillip Evans from MIT Lincoln Laboratory. The NiTi ribbon was provided by Nitinol Devices and Components. Financial support for this research was provided by the member organizations of the Smart Vehicle Concepts Center (<http://www.SmartVehicleCenter.org>), a National Science Foundation Industry/University Cooperative Research Center (I/UCRC). R.H. was partially supported by a Smart Vehicle Concepts Graduate Fellowship.

References

- [1] Vokoun D, Kafka V, Hu C. Recovery stresses generated by NiTi shape memory wires under different constrain conditions. *Smart Mater Struct* 2003;12:680–5.
- [2] Tsoi KA, Schrooten J, Zheng Y, Stalmans R. Part I. Thermomechanical characteristics of shape memory alloys. *Mater Sci Eng A* 2004;368:286–98.
- [3] De Vries E. Mechanics and mechanisms of ultrasonic metal welding. Ph.D. thesis. Columbus (OH): The Ohio State University; 2004.
- [4] Graff K. New developments in advanced welding. Cambridge (UK): Woodhead Publishing Limited; 2005 [chapter Ultrasonic Metal Welding].
- [5] Ram GDJ, Yang Y, Stucker BE. Effect of process parameters of bond formation during ultrasonic consolidation of aluminum alloy 3003. *J Manuf Syst* 2006;25(3):221–38.
- [6] Yang Y, Ram GDJ, Stucker BE. Bond formation and fiber embedment during ultrasonic consolidation. *J Mater Process Technol* 2009;209:4915–24.
- [7] Yang Y, Stucker BE, Ram GDJ. Mechanical properties and microstructures of SiC fiber-reinforced metal matrix composites made using ultrasonic consolidation. *J Compos Mater* 2010;44(26):3179–94.
- [8] Kong C, Soar R. Fabrication of metal-matrix composites and adaptive composites using ultrasonic consolidation process. *Mater Sci Eng A* 2005;412:12–8.
- [9] Shirzadi AA, Assadi H, Wallach ER. Interface evolution and bond strength when diffusion bonding materials with stable oxide films. *Surf Interface Anal* 2001;431:609–18.
- [10] Schick D. Characterization of aluminum 3003 ultrasonic additive manufacturing. Master's thesis. Columbus (OH): The Ohio State University; 2009.
- [11] Hopkins CD. Development and characterization of optimum process parameters for metallic composites made by ultrasonic consolidation. Master's thesis. Columbus (OH): The Ohio State University; 2010.
- [12] Truog AD. Bond improvement of Al/Cu joints created by very high power ultrasonic additive manufacturing. Master's thesis. Columbus (OH): The Ohio State University; 2012.
- [13] Zhang C, Li L. A coupled thermal–mechanical analysis of ultrasonic bonding mechanism. *Metall Mater Trans B* 2009;40B:196–207.
- [14] Yang Y, Ram GDJ, Stucker BE. Enhanced diffusion and phase transformation during ultrasonic welding of zinc and aluminum. *Scripta Mater* 2005;52:939–43.
- [15] Wu M. Fabrication of Nitinol materials and components. In: Proceedings of the international conference on shape memory and superelastic technologies; 2001. p. 258–92.
- [16] Wang G. Welding of Nitinol to stainless steel. In: Proceedings of the international conference on shape memory and super elastic technologies; 1997. p. 131–6.
- [17] Falvo A, Furgiuele F, Maletta C. Laser welding of a Ni Ti alloy: mechanical and shape memory behaviour. *Mater Sci Eng A* 2005;412:235–40.
- [18] Falvo A, Furgiuele F, Maletta C. Functional behaviour of a NiTi-welded joint: two-way shape memory effect. *Mater Sci Eng A* 2008;481–482:647–50.
- [19] Sittner P, Vokoun D, Dayananda GN, Stalmans R. Recovery stress generation in shape memory $\text{Ti}_{50}\text{Ni}_{45}\text{Cu}_5$ thin wires. *Mater Sci Eng A* 2000;286:298–311.
- [20] Zheng YJ, Schrooten J, Tsoi KA, Sittner P. Qualitative and quantitative evaluation of the interface in activated shape memory alloy composites. *Exp Mech* 2003;43(2):194–200.
- [21] Zheng YJ, Schrooten J, Tsoi KA, Stalmans R. Thermal response of glass fiber/epoxy composites with embedded TiNiCu alloy wires. *Mater Sci Eng A* 2002;335:157–63.
- [22] Zheng YJ, Cui LS, Schrooten J. Basic design guidelines for SMA/epoxy smart composites. *Mater Sci Eng A* 2005;390:139–43.
- [23] Brinson L. One dimensional constitutive behavior of shape memory alloys. *J Intell Mater Syst Struct* 1993;4(2):229–42.
- [24] Johnson Matthey. Nitinol technical specifications: transformation, physical, electrical, magnetic and mechanical; 2012. <<http://jmmmedical.com/index.php?p=resources&id=221>>.
- [25] Nitinol devices & components, material data sheet: Nitinol SM495 wire; 2009. <<http://www.nitinol.com/wp-content/uploads/2012/01/Material-Data-Sheet-Shape-Memory.pdf>>.
- [26] Lagoudas DC. Shape memory alloys. New York (NY): Science and Business Media, LLC; 2008.
- [27] Kaufman J, editor. Properties of aluminum alloys: tensile, creep, and fatigue data at high and low temperatures. Materials Park (OH): The Aluminum Association, Inc. and ASM International; 1999.
- [28] Kaufman J. Aluminum alloy database; 2009. <http://www.knovel.com.proxy.lib.ohio-state.edu/web/portal/browse/display?_EXT_KNOVEL_DISPLAY_bookid=844&VerticalID=0>.
- [29] Zheng Y, Cui L, Schrooten J. Temperature memory effect of a nickel–titanium shape memory alloy. *Appl Phys Lett* 2004;84(1):31–3.
- [30] Sittner P, Michaud V, Schrooten J. Modeling and material design of SMA polymer composites. *Mater Trans* 2002;43(5):984–93.
- [31] Sittner P, Stalmans R. Developing hybrid polymer composites with embedded shape-memory alloy wires. *JOM* 2000;52(10):15–20.
- [32] Sittner P, Stalmans R, Tokuda M. An algorithm for prediction of the hysteretic responses of shape memory alloys. *Smart Mater Struct* 2000;9(4):452–65.
- [33] Shetty DK. Shear-lag analysis of fiber push-out (indentation) tests for estimating interfacial friction stress in ceramic-matrix composites. *Commun Am Ceram Soc* 1988;71(2):107–9.